



Scanning electron microscopy characterization of structural features in suspended and non-suspended graphene by customized CVD growth



Jaesung Lee¹, Xuqian Zheng¹, Robert C. Roberts, Philip X.-L. Feng*

Department of Electrical Engineering & Computer Science, Case School of Engineering, Case Western Reserve University, 10900 Euclid Avenue, Cleveland, OH 44106, USA

ARTICLE INFO

Available online 3 December 2014

Keywords:

Scanning electron microscopy
Chemical vapor deposition
Suspended graphene
Membrane bulging
Folding lines
Wrinkles

ABSTRACT

We report an improved recipe for synthesizing high quality graphene through chemical vapor deposition (CVD), scanning electron microscopy (SEM) characterization of CVD graphene, and optimized SEM imaging conditions for efficient visualization of surface features in CVD graphene. We have developed an optimized graphene growth recipe by characterizing the quality of as-grown graphene using Raman spectroscopy and SEM. We have examined graphene samples both on copper (Cu) and silicon dioxide (SiO₂) substrate using SEM. We have found that features on the samples are highly sensitive to both SEM imaging conditions and the type of detector used. With low acceleration voltage (1 keV), immersion lenses, and through the lens detector, we have clearly observed fine features including wrinkles, folding lines, defects, and different layer numbers of graphene, many of which are not visible in un-optimized SEM images. Further, we demonstrate mechanical bulging of suspended CVD graphene membranes covering microtrenches by using electron beam to activate the trapped gas underneath. Our findings and techniques can lead to improved characterization, understanding, and manipulation of graphene and other two-dimensional materials.

© 2014 Elsevier B.V. All rights reserved.

1. Introduction

Graphene, a two-dimensional (2D) hexagonal carbon crystalline sheet, has attracted extensive attention since its discovery [1]. To date, chemical vapor deposition (CVD) [2,3] holds promise in producing large scale high-quality graphene for industrial applications [3]. Many attempts of growing large area single layer graphene (SLG) have been made. Besides SLG, polycrystalline graphene also has excellent mechanical properties comparable to that of SLG [4]. Moreover, wafer-scale continuous polycrystalline graphene films can be easily grown, showing that polycrystalline graphene has great potential for future applications such as nano- and micro-electromechanical systems (NEMS and MEMS) [5]. For characterizing quality, number of layers, defects, and atomic structures of graphene, many techniques such as atomic force microscopy (AFM) [2], transmission electron microscopy (TEM) [6] and Raman spectroscopy [7] have been employed. Among the many characterization methods, scanning electron microscopy (SEM) is a non-contact, mostly non-destructive, and comparatively more convenient and efficient tool for fast imaging, making it highly attractive for characterizing micro- and nano-scale features of graphene including wrinkles, folding lines, and grain shapes, especially for CVD grown graphene. However, due to its atomically thin structure, graphene is transparent to high

acceleration voltage SEM and it has been challenging to make SEM as a powerful tool for imaging graphene, especially at the device level, for engineered graphene structures and devices. Generally, attaining detailed structural features in imaging graphene devices has been more difficult than in devices made of more conventional materials or structures (e.g., nanowires, top-down lithographically defined NEMS devices) [8,9].

In this work, we have examined a set of varied CVD growth experiments to synthesize high quality and continuous graphene on copper (Cu) foils. The resulting films are carefully measured and compared to identify optimal growth parameters. Then, together with Raman spectroscopy, SEM imaging has been conducted on both suspended and non-suspended CVD graphene. We provide insight into the best set of imaging parameters for characterizing graphene features using SEM by comparing SEM images with different operating conditions, namely, electron energy and type of detectors, for different graphene structural features.

2. Graphene growth on Cu

We performed graphene synthesis with a home-built chemical vapor deposition system (Fig. 1). Using this system, a variety of CVD growth recipes have been explored to yield uniform and continuous large area graphene films. The resulted samples have been characterized using Raman and SEM observations, to establish optimized CVD growth parameters.

* Corresponding author.

E-mail address: philip.feng@case.edu (P.X.-L. Feng).

¹ Equally contributed authors.

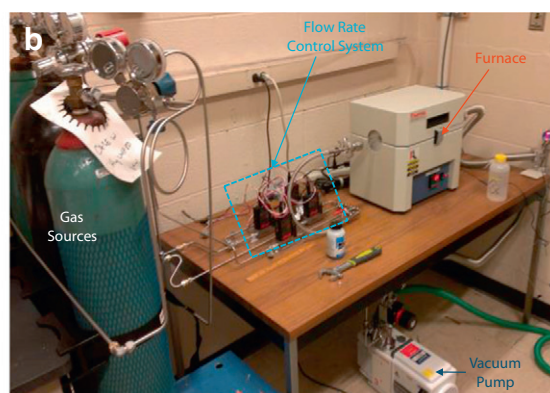
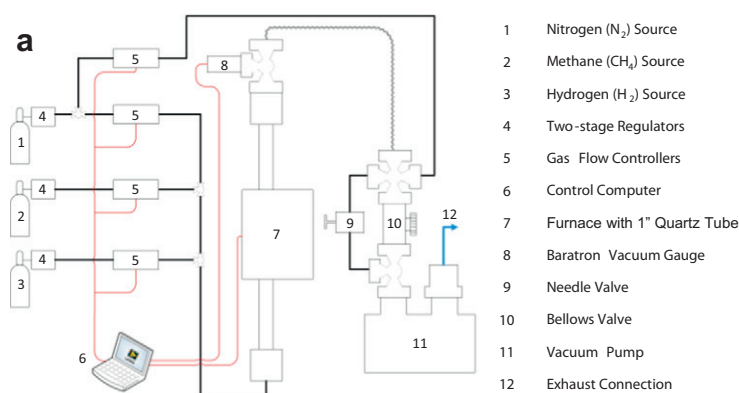


Fig. 1. The home-built CVD synthesis system used for the graphene growth. (a) A detailed illustration of the graphene CVD system design. Major components of the system are identified by numbers. (b) A photograph of the graphene CVD system with components labeled.

2.1. Graphene growth processes

We synthesized graphene on 25 μm -thick Alfa Aesar 99.8% Cu foils [2]. The CVD growth chamber was comprised of a 1-inch diameter quartz tube in a horizontal split-tube furnace. Computer programmed gas flows were obtained by using the mass flow controllers (Alicat Scientific) and the vacuum pressure level was monitored via a capacitive manometer gauge (Fig. 1a). Before synthesis, Cu foils were cut into $\sim 1\text{ cm} \times \sim 1\text{ cm}$ squares and chemically cleaned using acetic acid at 35 $^{\circ}\text{C}$ for 15 min, which removed copper oxide on Cu foil surfaces [10]. Then, two pieces of cleaned Cu substrates were introduced to the center position of the quartz tube. A vacuum pump was used to achieve $\sim 5\text{ mTorr}$ base pressure in the tube.

Upon completing the preparation steps, the growth process consists of three major steps: pre-annealing, graphene synthesis, and cooling down (Fig. 2). For the pre-annealing part, a 6 sccm hydrogen (H_2) gas flow was introduced, as the growth tube was heated to 1000 $^{\circ}\text{C}$. Once the set temperature had been reached, pre-annealing of the Cu substrates was conducted for 60 min, which stabilized the temperature of substrates, further cleaned Cu surfaces [11,12], and generated larger Cu grains by merging small ones. Next, graphene synthesis began by introducing methane (CH_4) gas to the tube as the carbon source. To determine the optimal CH_4 concentration, we conducted variable CH_4 flow rates (10 sccm, 30 sccm, and 50 sccm), along with constant H_2 flow rate (6 sccm), different chamber pressures (1 to 10 Torr) and growth durations (4 to 16 min). Detailed recipes are summarized in Table 1. After the growth step had been finished, the furnace was cooled down. Once temperature reached 200 $^{\circ}\text{C}$, CH_4 and H_2 flow was stopped and nitrogen (N_2) was introduced into the quartz tube. The Cu foils were then unloaded near room temperature, with synthesized graphene on them.

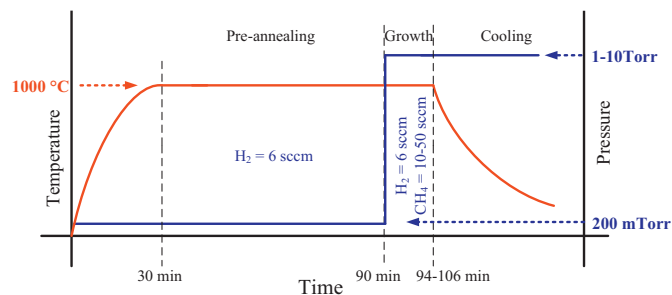


Fig. 2. A standard graphene CVD synthesis recipe (recipes #1–8 in Table 1), illustrated with temperature, duration and gas pressure used for each step. Red lines and blue lines show temperature and gas pressure in the tube during the growth, respectively.

2.2. Characterization of graphene for optimizing growth parameters

Using SEM and Raman spectroscopy, we examined multiple samples of graphene grown by different recipes. Raman spectra were recorded by a customized micro Raman setup. A 532 nm green laser was focused by a 100 \times optical microscope with a typical spot size on the sample of 1 μm . Before signal acquisition, the monochromator of the Raman system was calibrated by measuring an undoped silicon TO peak (520 cm^{-1}) for zero backlash. By comparing the images and Raman spectra, an optimized recipe of CVD synthesized graphene was obtained.

Fig. 3 shows examples of measured Raman spectra and SEM images of CVD graphene with different growth conditions. We found pronounced graphene G and 2D peaks from the Raman results. Regardless of graphene growth recipes, in majority of Raman results, full width at half maximum (FWHM) of the 2D peak are narrower than 32 cm^{-1} (Table 2), and the D peak (related to defect density of graphene) is either very small or invisible. These results indicate that the graphene samples synthesized by almost all of our CVD growth recipes are of high quality [13,14].

By using SEM, we have also observed surface morphology of CVD graphene grown by different growth recipes (as shown in Table 1). All SEM images in Fig. 3 were taken by using an FEI Helios NanoLab SEM with an Everhart-Thornley detector (ETD). In these SEM images, bright small clusters, typically $\sim 50\text{ nm}$, are visible. As the sizes of these clusters are much smaller than the Raman laser spot size ($\sim 1\text{ }\mu\text{m}$), it has been difficult to efficiently characterize these bright dots using Raman spectroscopy when the cluster density is low. To identify these clusters, we intentionally introduced 10 sccm of forming gas (95% N_2 , 5% H_2) together with 30 sccm of CH_4 into the growth tube at 1000 $^{\circ}\text{C}$ for 3 h to increase the cluster density. As shown in Fig. 3g, clusters with the density of $\sim 30/\mu\text{m}^2$ are formed on Cu substrates, dense enough for Raman measurement. Fig. 3h shows the measured Raman spectrum

Table 1
Summary of graphene growth recipes examined in this study.

Recipe ID	Gas flow rate [sccm]	Chamber pressure [Torr]	Growth time [min]
1	$\text{H}_2 = 6, \text{CH}_4 = 30$	5	16
2	$\text{H}_2 = 6, \text{CH}_4 = 30$	2	16
3	$\text{H}_2 = 6, \text{CH}_4 = 30$	1	16
4	$\text{H}_2 = 6, \text{CH}_4 = 30$	1	10
5	$\text{H}_2 = 6, \text{CH}_4 = 30$	1	5
6	$\text{H}_2 = 6, \text{CH}_4 = 50$	2	16
7	$\text{H}_2 = 6, \text{CH}_4 = 10$	2	16
8	$\text{H}_2 = 6, \text{CH}_4 = 50$	10	4
9	$95\%\text{N}_2 + 5\%\text{H}_2 = 10, \text{CH}_4 = 30$	5	180

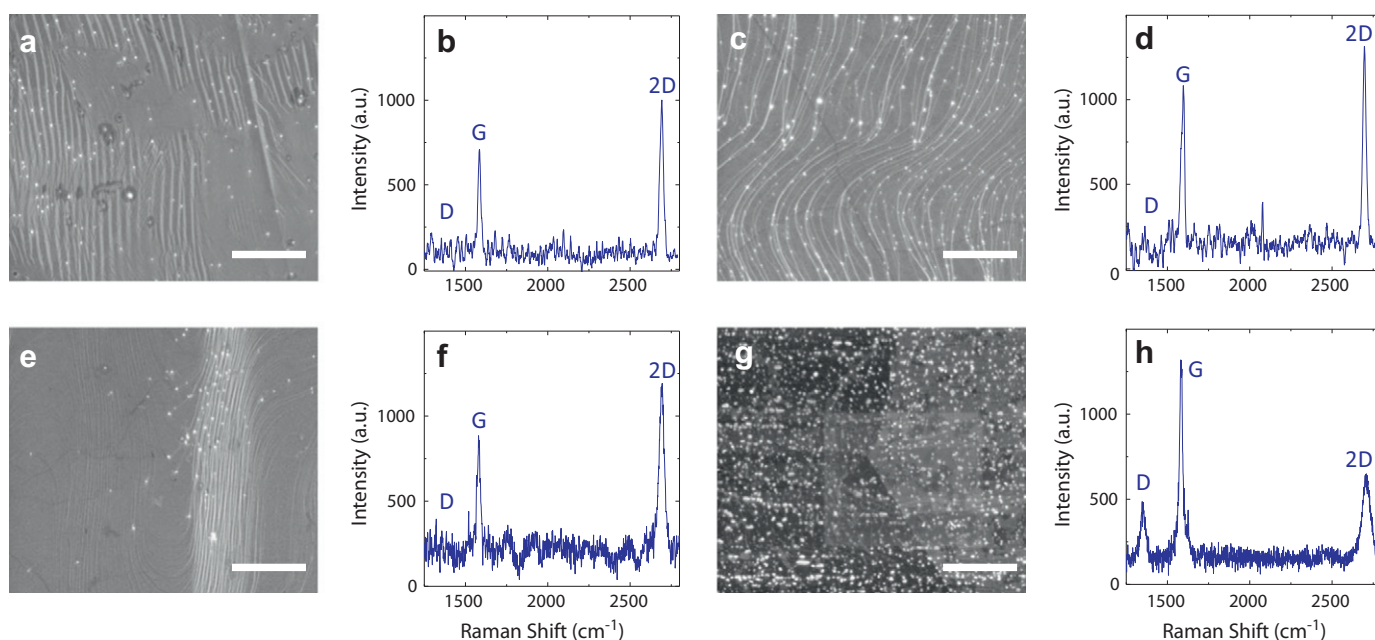


Fig. 3. CVD graphene with different growth conditions. SEM and Raman results of graphene grown using (a–b) recipe #3, (c–d) recipe #7, and (e–f) recipe #8. Also (g–h) SEM and Raman results of recipe used for high density carbon clusters forming. All the SEM images are taken by using 5 kV electron acceleration voltage and ETD. All scale bars are 3 μm .

focusing on bright clusters in SEM images. In contrast to the high quality graphene Raman spectra in Fig. 3b, d, and f, a high intensity of the D peak and low intensity of the 2D peak with broader FWHM ($\sim 70.0 \text{ cm}^{-1}$) were observed, suggesting that bright clusters in SEM images are 2D carbon structures with a larger number of layers. These carbon clusters are known as nucleation centers forming initial stages for graphene growth [11]. Impurities on Cu foil serve as nucleation sites in early stage of graphene growth due to their much lower nucleation barriers. While pure Cu does not adsorb carbon precursors, impurities on Cu foil have high super saturation of carbon precursors, resulting in multi-layered carbon cluster formation.

2.3. Graphene growth quality improvement

To reduce the density of carbon clusters and improve the film quality, optimization of the growth conditions was performed. First, the growth pressure dependence on the density of carbon cluster was examined. In the growth step, we fixed the gas flow rate (6 sccm for H_2 and 30 sccm for CH_4) and growth time (16 min), and varied chamber pressure from 1 Torr to 5 Torr (see recipes #1 – 3 in Table 1). As shown in Fig. 4a, the densities of carbon clusters are $1.78 \mu\text{m}^{-2}$, $1.56 \mu\text{m}^{-2}$ and $0.72 \mu\text{m}^{-2}$ when pressures are 1 Torr, 2 Torr and 5 Torr, respectively. The results suggest that higher growth pressure can

decrease the density of nucleation centers, allowing fewer carbon clusters to form during the growth. Similarly, a shorter growth time and lower H_2/CH_4 gas flow ratio are helpful to suppress the density of carbon clusters (Fig. 4b & c). Therefore, to achieve an optimized CVD graphene quality, we further increased the growth pressure to 10 Torr and shortened the growth time to 4 min, with a mixture of H_2 (6 sccm) and CH_4 (50 sccm) gas flow (see recipe #8). This yields high quality CVD graphene with low density of carbon clusters ($\sim 0.2 \mu\text{m}^{-2}$).

3. SEM characterization of CVD graphene on Cu foil

We have observed and compared surface features of CVD graphene (recipe #8) with various SEM imaging conditions to study surface features of CVD graphene. Through these investigations, we have determined optimized imaging conditions for graphene, which can also be applicable to other 2D materials.

3.1. Cu morphology

We have investigated Cu surface morphology using SEM. We have observed Cu evaporation when we introduced forming gas to the chamber. Fig. 5 shows SEM images of Cu substrate after 1000 $^\circ\text{C}$ pre-annealing for 60 min under 170 mTorr forming gas and subsequent 5 sccm of CH_4 gas flow at the same temperature for 30 min. From the SEM images, a noticeable amount of Cu is evaporated from the substrate, generating many terraces on the surface of the Cu foil. Evidently, downstream along the quartz tube, re-deposition of Cu on the quartz tube wall near its outlet was noticed. This Cu evaporation was only observed in Cu substrates with the forming gas process, suggesting that forming gas might not be well suited for pre-annealing for cleaning Cu surface.

Fig. 6a shows an optical microscope image of graphene on Cu substrates. In the image, Cu grain boundaries (GBs) and steps of grains are clearly visible. During the pre-annealing of Cu substrates, some small Cu grains merged into larger ones, known as grain coalescence. The typical size of small Cu grains is $\sim 80 \mu\text{m}$ while the typical size of merged Cu grains is around several millimeters. Steps and surface roughness of Cu grains were greatly reduced after coalescence, producing a relatively smooth and flat surface. Annealing time and temperature are key

Table 2
Summary of measured Raman spectra of graphene on Cu foil.

Recipe ID	D peak		G peak		2D peak	
	Position (cm^{-1})	FWHM (cm^{-1})	Position (cm^{-1})	FWHM (cm^{-1})	Position (cm^{-1})	FWHM (cm^{-1})
1	None		1584.8	20.0	2670.3	30.1
2	None		1592.0	23.8	2696.6	29.8
3	None		1588.2	20.4	2688.1	30.1
4	None		1586.6	20.1	2693.2	29.8
5	None		1589.2	19.5	2693.2	29.8
6	None		1588.2	19.2	2696.6	31.2
7	None		1593.3	24.2	2696.6	28.6
8	None		1581.0	18.2	2696.0	28.1
9	1351.1	46.1	1582.7	22.4	2704.4	70.0

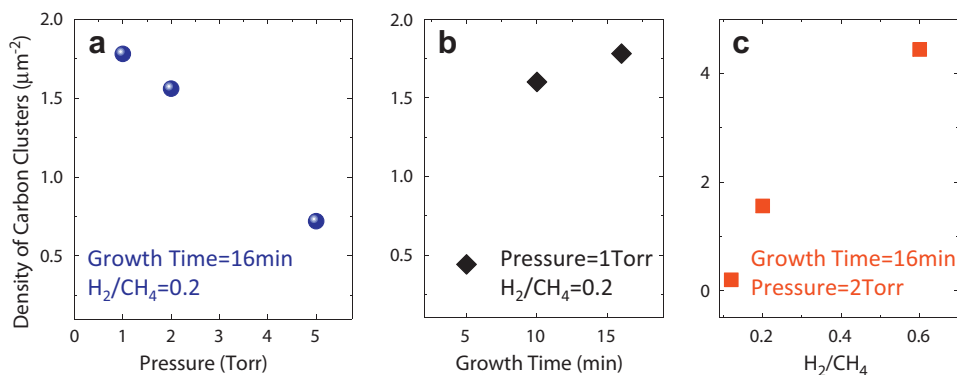


Fig. 4. Density of carbon clusters on graphene with different growth conditions (a) Chamber pressure dependency of carbon clusters. Graphene samples grown by recipes #1, #2, and #3 are examined. (b) Influence of growth time to the density of carbon dots. Data from recipes #3, #4, and #5 are used. (c) H_2/CH_4 gas flow rate dependency. Recipes #2, #6, and #7 are employed.

parameters for Cu grain coalescence. After 1000 °C and 60 min pre-annealing, unmerged small Cu grains and newly formed big grains were coexisting.

While some detailed surface morphological properties of the Cu substrate can be easily observed in an optical microscope, surface features of graphene are barely visible due to its high transparency. We therefore further characterized graphene on Cu substrates with SEM (FEI Helios NanoLab). Similar to optical microscope images, we observed Cu grains with low magnification SEM (Fig. 6b & c). In SEM images taken by a backscattering electron detector in Fig. 6b and Fig. 7a, Cu grains can be clearly identified by the contrast changes arisen from different grain orientations, which are less obvious in the ETD SEM image (Fig. 6c).

3.2. Graphene morphology

Besides Cu morphology, other kinds of features can be observed throughout the CVD grown graphene, e.g., dark lines. These dark lines are known as graphene folding lines. During growth, the thermal expansion coefficient for Cu is $16.3 \times 10^{-6} \text{ K}^{-1}$ at 300 K and $20 \times 10^{-6} \text{ K}^{-1}$ at 800 K [15], while graphene has mainly a negative thermal expansion coefficient ranging from $-7.9 \times 10^{-6} \text{ K}^{-1}$ to $4.35 \times 10^{-6} \text{ K}^{-1}$ [16–21]. This difference in the thermal expansion coefficient between graphene and the Cu substrate generates approximately 0.3–0.6% thermal strain in CVD grown graphene on Cu (111) [22]. This strain, however, is much lower than CVD graphene's intrinsic strain limit, which is as high as 20% [23]. In addition to the

mechanical properties, the electrical properties of CVD graphene are comparable to exfoliated graphene [24]; thus we believe that the small amount of defects generated is negligible and does not degrade intrinsic properties of graphene. The thermally induced stress lifts up some areas of graphene and thus makes narrow trilayer graphene folding lines [25,26]. We found that the contrast of folding lines depends significantly on SEM detector type. While folding lines are invisible on a backscattering electron SEM image (Fig. 7a), they are clearly observed in secondary electron SEM images collected by ETD and through the lens detector (TLD) with a magnetic immersion lens, where they appear as lower brightness compared to the brightness of monolayer graphene regions. Moreover, as shown in Fig. 7b and c, folding lines appear with better contrast in the SEM images taken with TLD than those taken with ETD. In addition to graphene folding lines, many dark spots (yellow circles in Fig. 7a–c) are also visible on the SEM images and these areas are few-layer graphene [27]. Few-layer graphene regions are visible in all three types of detectors. Similar to folding lines, TLD images provide the best contrast of the features. Since graphene is transparent to high energy electrons, most of backscattered electrons and secondary electrons are generated from the Cu substrate underneath the graphene. The generated electrons need to pass through graphene and be collected by SEM detectors, in a way that graphene can act as electron barriers to block some of the electrons emitted from Cu. As the number of graphene layers increases, more electrons generated from the substrate will be blocked, leading to lower brightness in SEM images.

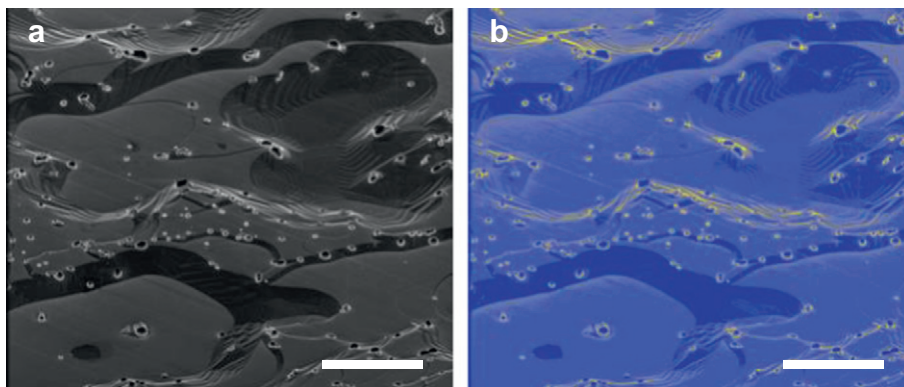


Fig. 5. 2 kV (a) original and (b) colored SEM images of Cu substrate with forming gas process. Many terraces are created due to Cu evaporation, as also evidenced by re-deposition of Cu on quartz tube wall downstream. Scales bars are 3 μm .

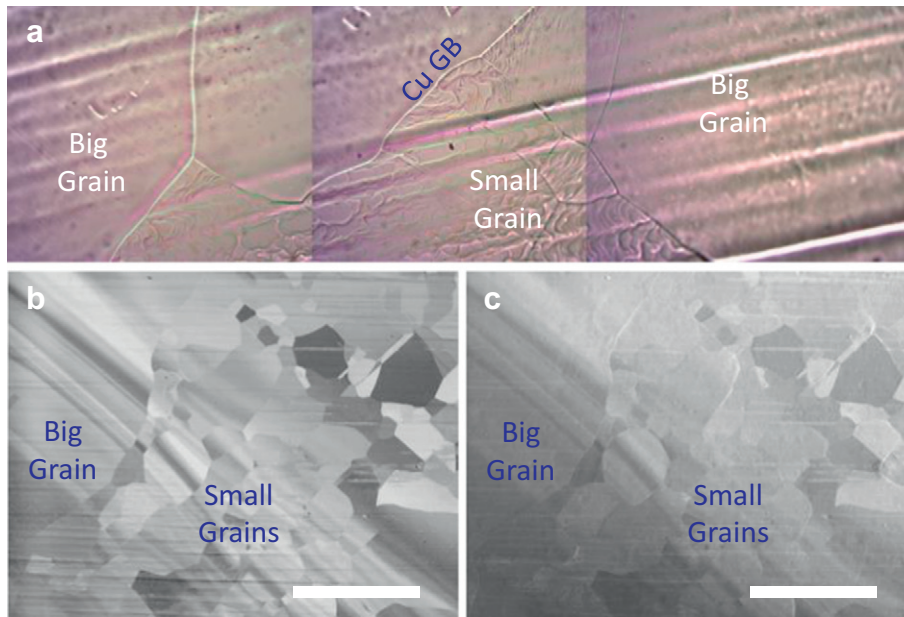


Fig. 6. (a) An optical microscope image of graphene on a Cu substrate. The image shows the shape and morphology of Cu grain after 1000 °C, 60 min pre-annealing along with CVD graphene synthesis. (b) & (c) Low magnification 5 kV SEM images of the same area of graphene on Cu with both (b) backscattering electron detector and (c) ETD. Big and small Cu grains are coexisting on the images. Scale bars are 300 μm in (b) & (c).

Thus, by calibrating their brightness, one could precisely identify the number of layers of graphene using only SEM [28].

3.3. Colored SEM images

The surface features of the CVD graphene in SEM images can be further clarified and easily identified by a software enhanced imaging process. Since SEM detectors are monochromatic, thus detected electrons from the sample are converted to the images only by using brightness and contrast to display information of the samples; sometimes captured graphene morphology properties are not clear enough to precisely identify appearances of surface features. By adding software assisted colors in these SEM images, surface morphology of the CVD graphene on Cu substrates can be further clarified. Fig. 8 shows SEM images before and after software enhancement. As shown in Fig. 8b, few-layer graphene regions and narrow folding lines on the CVD graphene can be clearly identified by different colors. In addition to graphene surface characteristics, details of Cu substrate morphology are also vividly enhanced.

3.4. Influence of electron acceleration voltage

To further investigate SEM imaging conditions, we lowered the electron acceleration energy from 5 kV to 1 kV and measured surface features of graphene on Cu foils produced by recipe #8, by employing TLD. As shown in Fig. 9b–h, numerous features appear comparing to SEM images in Fig. 7a–c, where typical SEM operating conditions were applied (5 kV electron acceleration voltage). Most prominently, folding lines are brighter than monolayer graphene in Fig. 9, which is clearly different than those in Fig. 7a–c. In addition, the contrast of folding lines is greatly enhanced, making them highly distinctive in SEM images. Besides folding lines, we found numerous of bright small spots on graphene in SEM images. These may be graphene defects such as discontinuities of carbon atoms, ruptures, and three-dimensional carbon structures, which may generate more secondary electrons. Moreover, as shown in Fig. 9b–e, these bright small features are denser in areas of graphene on small unmerged Cu grains than on large coalesced Cu grains, indicating a graphene quality reduction caused by Cu surface features, such as steps, terraces and rough surfaces. Therefore, we conclude that low electron acceleration voltage SEM can lead to smaller

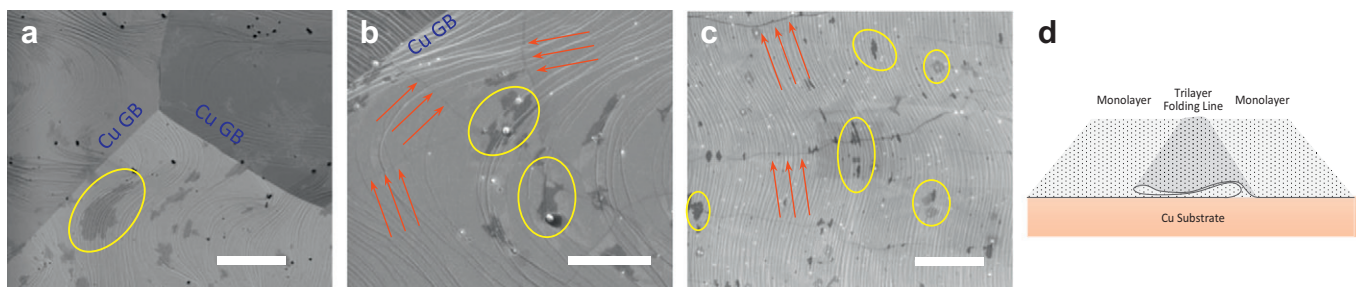


Fig. 7. 5 kV SEM images of graphene on Cu substrates with different detectors. High magnification SEM images using (a) backscattering detector (b) ETD, and (c) TLD. The red arrows indicate graphene folding lines, the yellow circles present multilayer graphene regimes, and each blue text of 'Cu GB' indicates a Cu grain boundary. Scale bars in (a)–(c) are 5 μm . (d) A schematic illustration of a folding line.

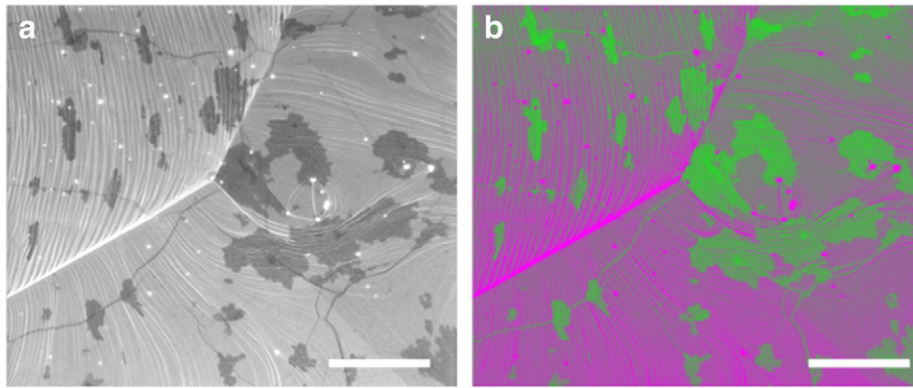


Fig. 8. Color-enhancement of an SEM image of graphene on Cu. (a) A 5 kV SEM image captured using TLD. (b) The software colored SEM image. Not only graphene features, but surface morphology of Cu substrate is also greatly enhanced. All scale bars are 5 μm .

penetration depth, and provide better morphological information of graphene, which is suitable for high-throughput characterization of all atomically thin two dimensional materials.

4. SEM characterization of transferred graphene

We transferred our CVD graphene (recipe #8) onto SiO_2/Si substrates to further explore the structural features and quality of graphene. Under SEM, some different types of morphological characteristics were identified from the graphene on SiO_2/Si substrates.

4.1. Graphene transfer process

We transferred graphene, synthesized using recipe #8, from Cu foils onto 290 nm-thick- SiO_2 on Si substrate, with both flat/blank substrates and pre-patterned structures [29,30]. Since atomically thin graphene

can be easily damaged during the transfer process, polymethyl methacrylate (PMMA) was coated on the graphene side of the graphene/Cu foil substrate for protection and support purposes. Next, we gently put the PMMA/graphene/Cu sandwich into $\text{Fe}(\text{NO}_3)_3$ solution (1 M) with PMMA side up in order to etch away Cu foil completely (Fig. 10b). The remaining PMMA/graphene heterostructure floated in the Cu etchant solution because PMMA is light and hydrophobic. Following the Cu etching process, PMMA/graphene structures were carefully scooped and rinsed in deionized (DI) water to wash away remaining Cu etchant solution (Fig. 10d). To ensure that the sample is etchant free, the rinse step was repeated 6 times. Then, we dipped the 290 nm- SiO_2 -on-Si substrate into DI water and placed the PMMA/graphene structures onto the desired position of the substrate (Fig. 10e). The free standing side of graphene surface adhered to the SiO_2/Si substrate by van der Waals forces. After drying, the PMMA support was removed by acetone and isopropyl alcohol (IPA). The resulting graphene region has clearly

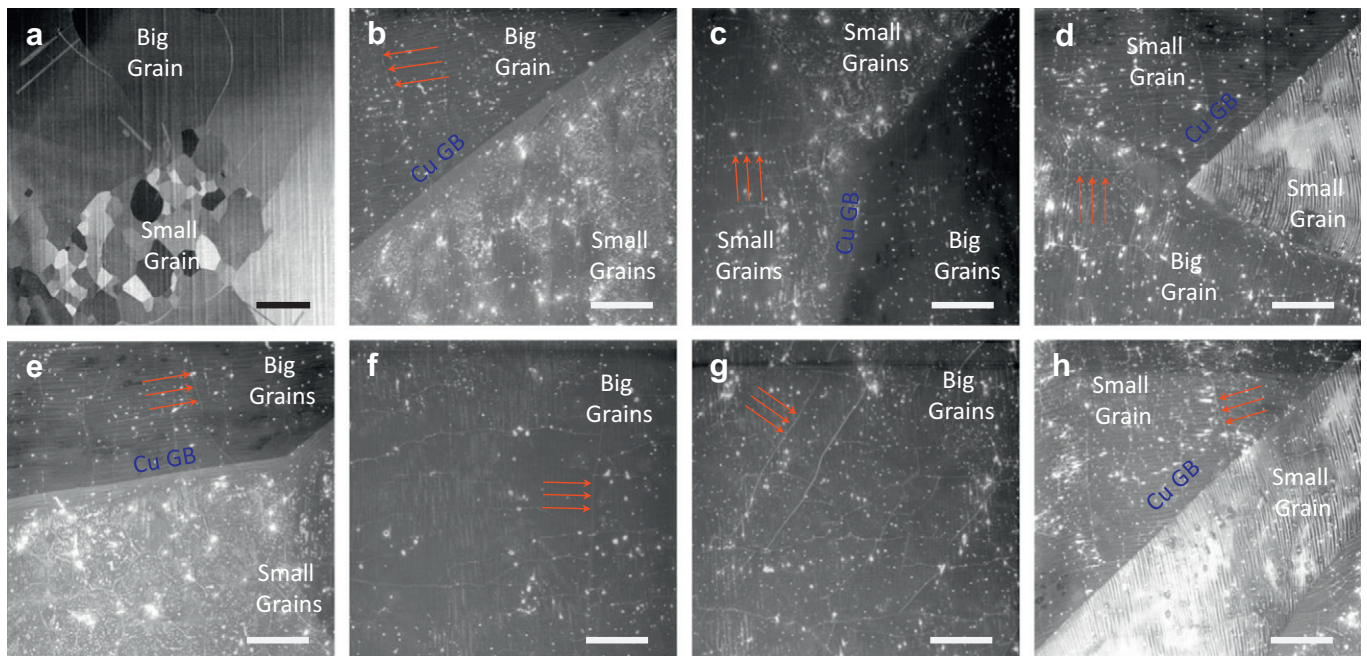


Fig. 9. 1 kV SEM images of graphene on Cu substrates with different detectors. (a) Low magnification SEM images with ETD detectors. Scale bar is 200 μm . (b)–(h) High magnification SEM images with TLD detectors. The red arrows indicate graphene folding lines and each blue text of 'Cu GB' indicates a Cu grain boundary. Scale bars in (b)–(h) are 5 μm .

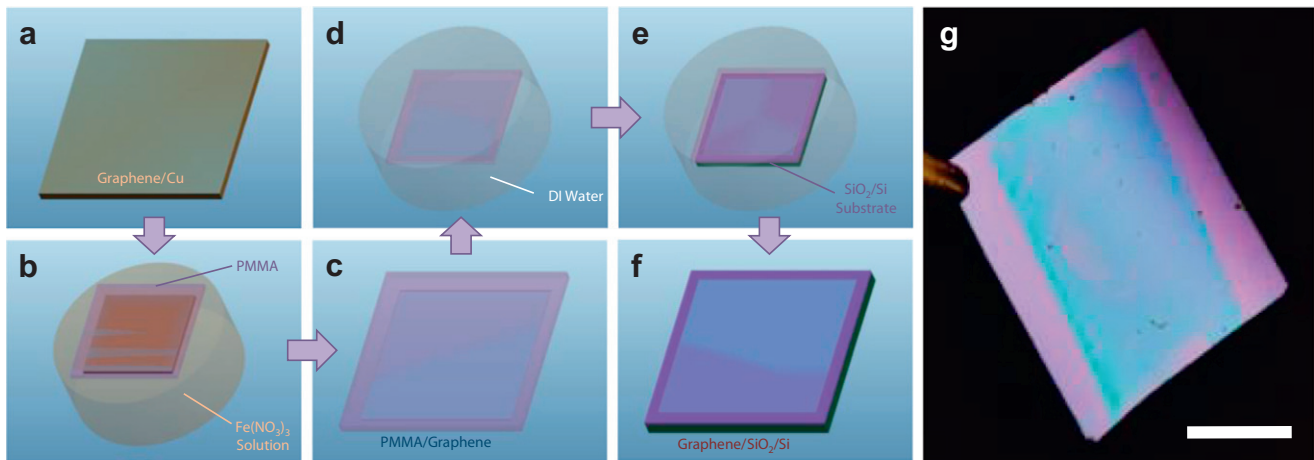


Fig. 10. Graphene transfer. (a)–(f) A schematic illustration of our graphene transfer processes. (a) Graphene synthesized on Cu foil. (b) Graphene/Cu substrate coated with PMMA in $\text{Fe}(\text{NO}_3)_3$ solution. (c) Graphene on PMMA. (d) Cu etchant solution cleaning using DI water. (e) Contacting SiO_2/Si substrate with graphene on PMMA in DI water. (f) Final sample by removing PMMA using acetone and IPA. (g) Photograph of transferred CVD graphene on the flat 290nm- SiO_2 -on-Si substrate. Scale bar is 1 cm. Graphene is visible by color and contrast.

different color and contrast compared to bare SiO_2/Si substrate, making graphene visible with the naked eyes (Fig. 10 g) [31].

4.2. Quality of graphene on SiO_2 substrate

We examined the quality of graphene transferred on 290 nm- SiO_2 -on-Si substrates by performing Raman spectroscopy on various spots (Fig. 11). Raman data from four different positions clearly demonstrate very small D peak, sharp 2D peak (with FWHM $\sim 30 \text{ cm}^{-1}$), showing high quality of the sample after the wet transfer process. Moreover, all

measured Raman spectra are almost exactly the same, indicating great uniformity of transferred CVD graphene.

4.3. Morphology of non-suspended graphene on SiO_2 substrate

While optical microscope images and Raman results demonstrate that transferred graphene is continuous and of high quality, SEM images reveal new features of the CVD graphene on SiO_2 . Besides dark graphene folding lines, narrow bright lines were found in the transferred graphene on SiO_2 (Fig. 12). As shown in Fig. 12a, these lines are wrinkles

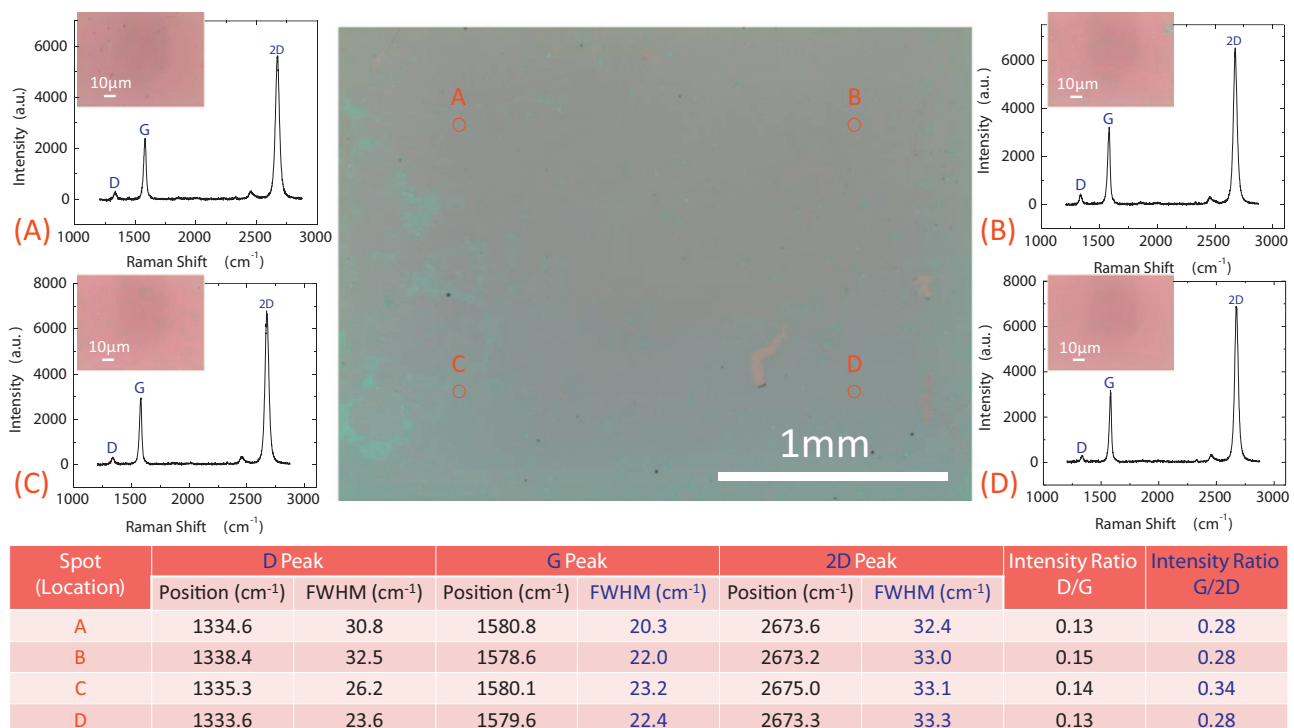


Fig. 11. Summary of Raman measurements taken at various locations across CVD graphene transferred onto SiO_2 . The table summarizes measured D, G, 2D Raman peaks.

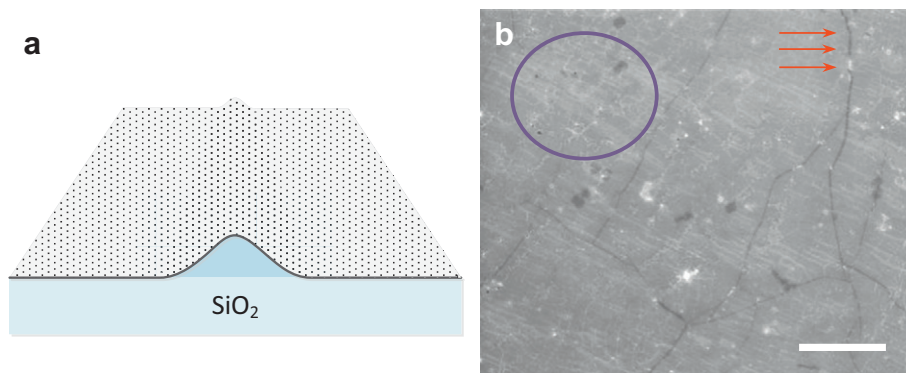


Fig. 12. Transferred graphene on 290 nm-SiO₂-on-Si substrate. (a) An illustration of a graphene wrinkle. (b) 5 kV SEM images of transferred graphene on the SiO₂/Si substrate using a TLD. The red arrows indicate a graphene folding line and the violet circle marks the region with many graphene wrinkles. Scale bar is 5 μm.

in graphene [26,32] which were introduced during the transfer process. These results suggest that SEM is a powerful tool for identifying nano-scale surface roughness in transferred graphene which cannot be easily detected by Raman spectroscopy.

4.4. Morphology of suspended graphene on SiO₂ substrate

We fabricated suspended graphene structures using the same wet transfer process in Section 4.1 and investigated their surface morphological characteristics with SEM (Fig. 13). In the images, clear contrast was observed between the suspended and non-suspended areas. As shown in Fig. 13a and b for circular drumhead graphene membranes,

residues of PMMA can be clearly observed on the suspended graphene areas, while on non-suspended areas, they become less obvious. Similar contrast was observed in side-view SEM images of graphene suspended across triangular trenches (Fig. 13c & d). This process is useful for making suspended devices such as two-dimensional vibrating mechanical resonators [33].

Finally, we have demonstrated non-contact, in-situ mechanical manipulation of suspended graphene using SEM. Interestingly, we have observed bulging of suspended circular graphene drumheads induced by electron beam irradiation (Fig. 14). When the sample of transferred graphene membranes covering circular microtrenches was loaded into the SEM for examination, initially the membranes were mostly

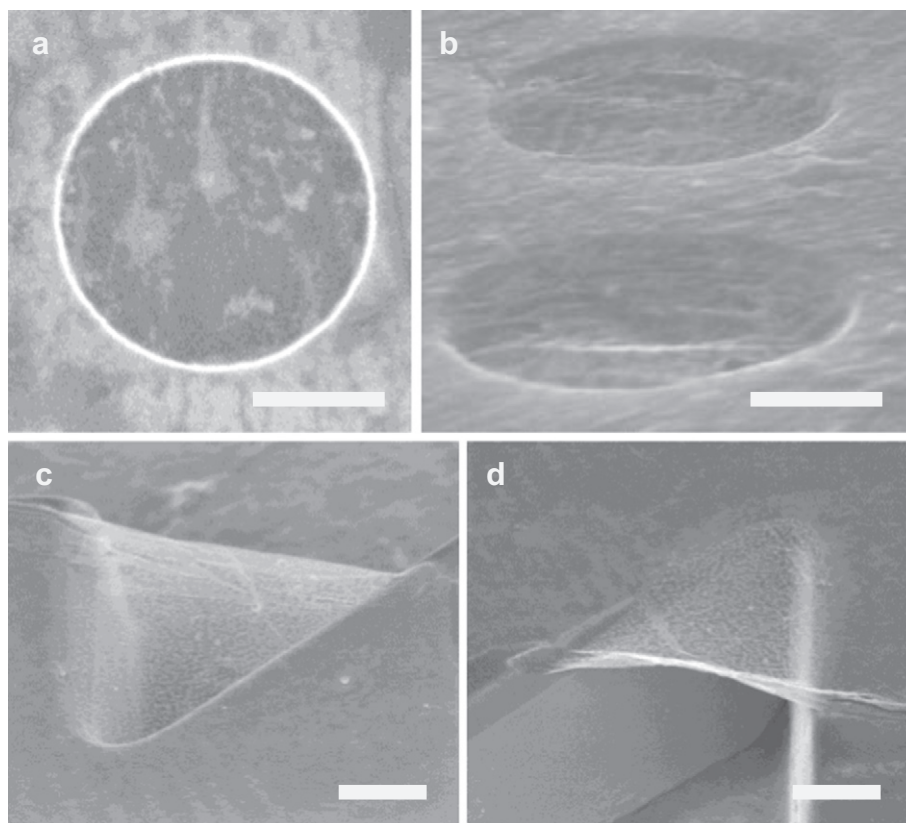


Fig. 13. Suspended CVD graphene on the pre-patterned 290 nm-SiO₂-on-Si substrates. (a) A Top view, and (b) 45 degree tilted SEM image of circular drumhead graphene. (c)–(d) 52 degree tilted view SEM images of graphene on triangular trenches, measured with 2 kV electron acceleration voltage with the TLD. All scale bars are 1 μm.

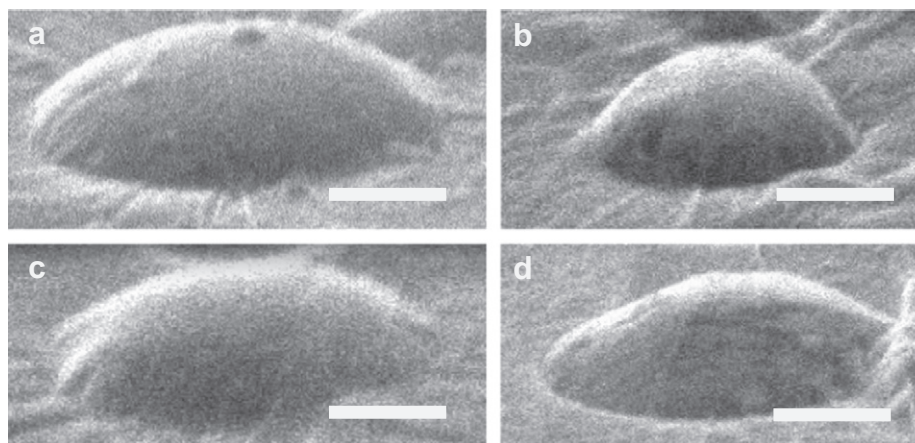


Fig. 14. SEM snapshot images (from real-time video during in-situ measurement). Examples of membrane bulging of transferred CVD graphene under electron beam irradiation in the SEM. All scale bars are 1 μm .

collapsed to the bottom of the trenches, and a small population of membranes were free-standing flat. They remain in such status in SEM vacuum after the SEM imaging started and when the magnification was low. As shown in Fig. 14, as we zoomed into small regions with increasing magnification, and focused the electron beam onto an individual transferred graphene membrane, we clearly observed that the collapsed membranes start to inflate and bulge up in real time, gradually achieving dome-shaped structures (images of Fig. 14 are directly taken from a video recorded during the SEM imaging). This intriguing bulging phenomenon immediately means that the focused electron beam irradiation has caused a pressure difference [34]. It suggests that the electron beam irradiation is effective in activating or exciting vapor or gas molecules trapped underneath the membranes, and adsorbates on various inner surfaces and corrugations inside the cavity, and thus ‘degassing’ the cavity, inducing pressure difference, and driving the bulging effect. These observations also suggest that such electron beam irradiation may be exploited to help salvage devices suffering from stiction, a well-known challenge in making one-/two-dimensional suspended structures out of liquid phase solutions and processes.

5. Conclusions

By examining the quality of graphene samples from different CVD growth conditions, we have determined a recipe for high quality CVD graphene synthesis. We show that SEM can be used for characterizing and identifying features (e.g., wrinkles, folding lines, defects, numbers of layers, and wet transfer residues) in CVD graphene. Specifically, we show that low acceleration voltage SEM with the TLD detector is particularly suitable for imaging CVD graphene. We have further demonstrated releasing and bulging of CVD graphene membranes that were initially in stiction, by utilizing focused electron beam irradiation inside SEM.

Prime novelty statement

We report an improved recipe for synthesizing high-quality graphene through chemical vapor deposition (CVD), scanning electron microscopy (SEM) characterization of CVD graphene, and optimized SEM imaging conditions for efficient visualization of surface features in CVD graphene.

Acknowledgments

We thank A. Avishai, L. Zhao, and Z. Wang for helpful discussions and technical support in the labs. We acknowledge the support from the

Case School of Engineering and the National Academy of Engineering (NAE) Grainger Foundation Frontiers of Engineering (FOE) Award (FOE 2013-005).

References

- [1] K.S. Novoselov, Nobel lecture: graphene: materials in the flatland, *Rev. Mod. Phys.* 83 (2011) 837–849.
- [2] X. Li, W. Cai, J. An, S. Kim, J. Nah, D. Yang, R. Piner, A. Velamakanni, I. Jung, E. Tutuc, S.K. Banerjee, L. Colombo, R.S. Ruoff, Large-area synthesis of high-quality and uniform graphene films on copper foils, *Science* 324 (2009) 1312–1314.
- [3] S. Bae, H. Kim, Y. Lee, X. Xu, J.-S. Park, Y. Zheng, J. Balakrishnan, T. Lei, H. Ri, H.R. Kim, Y.I. Song, Y.-J. Kim, K.S. Kim, B. Özyilmaz, J.-H. Ahn, B.H. Hong, S. Iijima, Roll-to-roll production of 30-inch graphene films for transparent electrodes, *Nat. Nanotechnol.* 5 (2010) 574–578.
- [4] H.I. Rasool, C. Ophus, W.S. Klug, A. Zettl, J.K. Gimzewski, Measurement of the intrinsic strength of crystalline and polycrystalline graphene, *Nat. Commun.* 4 (2013) 2811.
- [5] A.M. van der Zande, R.A. Barton, J.S. Alden, C.S. Ruiz-Vargas, W.S. Whitney, P.H.Q. Pham, J. Park, J.M. Parpia, H.G. Craighead, P.L. McEuen, Large-scale arrays of single-layer graphene resonators, *Nano Lett.* 10 (2010) 4869–4873.
- [6] J.C. Meyer, A.K. Geim, M.I. Katsnelson, K.S. Novoselov, T.J. Booth, S. Roth, The structure of suspended graphene sheets, *Nature* 446 (2007) 60–63.
- [7] A.C. Ferrari, J.C. Meyer, V. Scardaci, C. Casiraghi, M. Lazzeri, F. Mauri, S. Piscanec, D. Jiang, K.S. Novoselov, S. Roth, A.K. Geim, Raman spectrum of graphene and graphene layers, *Phys. Rev. Lett.* 97 (2006) 187401.
- [8] X.L. Feng, R. He, P. Yang, M.L. Roukes, Very high frequency silicon nanowire electro-mechanical resonators, *Nano Lett.* 7 (2007) 1953–1959.
- [9] X.M.H. Huang, X.L. Feng, C.A. Zorman, M. Mehregany, M.L. Roukes, VHF, UHF and microwave frequency nanomechanical resonators, *New J. Phys.* 7 (2005) 247.
- [10] K.L. Chavez, D.W. Hess, A novel method of etching copper oxide using acetic acid, *J. Electrochem. Soc.* 148 (2001) G640–G643.
- [11] H. Wang, G. Wang, P. Bao, S. Yang, W. Zhu, X. Xie, W. Zhang, Controllable synthesis of submillimeter single-crystal monolayer graphene domains on copper foils by suppressing nucleation, *J. Am. Chem. Soc.* 134 (2012) 3627–3630.
- [12] A. Mohsin, L. Liu, P. Liu, W. Deng, I.N. Ivanov, G. Li, O.E. Dyck, G. Duscher, J.R. Dunlap, K. Xiao, G. Gu, Synthesis of millimeter-size hexagon-shaped graphene single crystals on resolidified copper, *ACS Nano* 7 (2013) 8924–8931.
- [13] A.C. Ferrari, Raman spectroscopy of graphene and graphite: disorder, electron–phonon coupling, doping and nonadiabatic effects, *Solid State Commun.* 143 (2007) 47–57.
- [14] A. Ismach, C. Druzgalski, S. Penwell, A. Schwartzberg, M. Zheng, A. Javey, J. Bokor, Y. Zhang, Direct chemical vapor deposition of graphene on dielectric surfaces, *Nano Lett.* 10 (2010) 1542–1548.
- [15] F.C. Nix, D. MacNair, The thermal expansion of pure metals: copper, gold, aluminum, nickel, and iron, *Phys. Rev.* 60 (1941) 597–605.
- [16] M. Pozzo, D. Alfè, P. Lacovig, P. Hofmann, S. Lizzit, A. Baraldi, Thermal expansion of supported and freestanding graphene: lattice constant versus interatomic distance, *Phys. Rev. Lett.* 105 (2011) 135501.
- [17] K.V. Zakharchenko, M.I. Katsnelson, A. Fasolino, Finite temperature lattice properties of graphene beyond the quasiharmonic approximation, *Phys. Rev. Lett.* 102 (2009) 046808.
- [18] D. Yoon, Y.-W. Son, H. Cheong, Negative thermal expansion coefficient of graphene measured by Raman spectroscopy, *Nano Lett.* 11 (2011) 3227–3231.
- [19] W. Pan, J. Xiao, J. Zhu, C. Yu, G. Zhang, Z. Ni, K. Watanabe, T. Taniguchi, Y. Shi, X. Wang, Biaxial compressive strain engineering in graphene/boron nitride heterostructures, *Sci. Rep.* 2 (2012) 893.

- [20] J.-W. Jiang, J.-S. Wang, B. Li, Thermal expansion in single-walled carbon nanotubes and graphene: nonequilibrium Green's function approach, *Phys. Rev. B* 80 (2009) 205429.
- [21] W. Bao, F. Miao, Z. Chen, H. Zhang, W. Jang, C. Dames, C.N. Lau, Controlled ripple texturing of suspended graphene and ultrathin graphite membranes, *Nat. Nanotechnol.* 4 (2009) 562–566.
- [22] R. He, L. Zhao, N. Petrone, K.S. Kim, M. Roth, J. Hone, P. Kim, A. Pasupathy, A. Pinczuk, Large physisorption strain in chemical vapor deposition of graphene on copper substrates, *Nano Lett.* 12 (2012) 2408–2413.
- [23] G.-H. Lee, R.C. Cooper, S.J. An, S. Lee, A. van der Zande, N. Petrone, A.G. Hammerberg, C. Lee, B. Crawford, W. Oliver, J.W. Kysar, J. Hone, High-strength chemical-vapor-deposited graphene and grain boundaries, *Science* 340 (2013) 1073–1075.
- [24] N. Petrone, C.R. Dean, I. Meric, A.M. van der Zande, P.Y. Huang, L. Wang, D. Muller, K.L. Shepard, J. Hone, Chemical vapor deposition-derived graphene with electrical performance of exfoliated graphene, *Nano Lett.* 12 (2012) 2751–2756.
- [25] K. Kim, Z. Lee, B.D. Malone, K.T. Chan, B. Aleman, W. Regan, W. Gannett, M.F. Crommie, M.L. Cohen, A. Zettl, Multiply folded graphene, *Phys. Rev. B* 83 (2011) 245433.
- [26] W. Zhu, T. Low, V. Perebeinos, A.A. Bol, Y. Zhu, H. Yan, J. Tersoff, P. Avouris, Structure and electronic transport in graphene wrinkles, *Nano Lett.* 12 (2012) 3431–3436.
- [27] L. Brown, R. Hovden, P. Huang, M. Wojcik, D.A. Muller, J. Park, Twinning and twisting of tri- and bilayer graphene, *Nano Lett.* 12 (2012) 1609–1615.
- [28] H. Hiura, H. Miyazaki, K. Tsukagoshi, Determination of the number of graphene layers: discrete distribution of the secondary electron intensity stemming from individual graphene layers, *Appl. Phys. Express* 3 (2010) 095101.
- [29] J.W. Suk, A. Kitt, C.W. Magnuson, Y. Hao, S. Ahmed, J. An, A.K. Swan, B.B. Goldberg, R.S. Ruoff, Transfer of CVD-grown monolayer graphene onto arbitrary substrates, *ACS Nano* 5 (2011) 6916–6924.
- [30] J. Lee, P.X.-L. Feng, High frequency graphene nanomechanical resonators and transducers, *Proc. IEEE Int. Freq. Control Symp. (IFCS 2012)* 2012, <http://dx.doi.org/10.1109/IFCS.2012.6243742> (Baltimore, MD, May 21–24).
- [31] P. Blake, E.W. Hill, A.H. Castro Neto, K.S. Novoselov, D. Jiang, R. Yang, T.J. Booth, A.K. Geim, Making graphene visible, *Appl. Phys. Lett.* 91 (2007) 063124.
- [32] J. Xie, J.P. Spallas, Different contrast mechanisms in SEM imaging of graphene, *Tech. Rep.* (2012) (Agilent Technologies).
- [33] J. Lee, Z. Wang, K. He, J. Shan, P.X.-L. Feng, High frequency MoS₂ nanomechanical resonators, *ACS Nano* 7 (2013) 6086–6091.
- [34] J. Lee, Z. Wang, K. He, J. Shan, P.X.-L. Feng, Air damping of atomically thin MoS₂ nanomechanical resonators, *Appl. Phys. Lett.* 105 (2014) 023104.